J Nanopart Res (2011) 13:5985–5997
DOI 10.1007/s11051-011-0346-7

SPECIAL ISSUE: NANOSTRUCTURED MATERIALS 2010

Electrochemical and hydrothermal deposition of ZnO on silicon: from continuous films to nanocrystals

M. Balucani · P. Nenzi · E. Chubenko · A. Klyshko · V. Bondarenko

Received: 4 October 2010 / Accepted: 12 March 2011 / Published online: 26 March 2011

Abstract This article presents the study of the electrochemical deposition of zinc oxide from the non-aqueous solution based on dimethyl sulfoxide and zinc chloride into the porous silicon matrix. The features of the deposition process depending on the thickness of the porous silicon layer are presented. It is shown that after deposition process the porous silicon matrix is filled with zinc oxide nanocrystals with a diameter of 10–50 nm. The electrochemically deposited zinc oxide layers on top of porous silicon are shown to have a crystalline structure. It is also shown that zinc oxide crystals formed by hydrothermal method on the surface of electrochemically deposited zinc oxide film demonstrate ultra-violet luminescence. The effect of the porous silicon layer thickness on the morphology of the zinc oxide is shown. The structures obtained demonstrated two luminescence bands peaking at the 375 and 600 nm wavelengths. Possible applications of ZnO nanostructures, porous and continuous polycrystalline ZnO films such as gas sensors, light-emitting diodes, photovoltaic devices, and nanopiezo energy generators are considered. Aspects of integration with conventional silicon technology are also discussed.

Keywords Zinc oxide · Porous silicon · Nanocrystal · X-ray diffraction · Photoluminescence

M. Balucani (✉) · P. Nenzi
Electronic Department, Sapienza Rome University, Via Eudossiana 18, Rome 18-00184, Italy
e-mail: Balucani@die.uniroma1.it

E. Chubenko · A. Klyshko · V. Bondarenko
Micro and Nanoelectronics Department, Belarusian State University of Informatics and Radioelectronics, P. Brovka Str. 6, Minsk 220013, Belarus

Introduction

This study is concerned on the technological issues in the growth of zinc oxide films and zinc oxide nanocrystals on the surface of silicon wafers with a porous silicon (PS) buffer layer.

Currently, silicon is the fundamental material in microelectronics and a broad set of electronic integrated circuits (IC), microelectromechanical systems (MEMS), nanoelectromechanical systems (NEMS), and opto-electronics devices are produced on silicon substrates. As predicted by International Technology Roadmap for Semiconductor, the prospects for single-crystal silicon IC, MEMS, NEMS, and opto-electronic production to 2025 year are quite well defined though not unclouded (ITRS 2009).

Because of indirect band gap structure of single-crystal silicon, its luminescence efficiency is very low (usually 10^{-4}%), so silicon-based light-emitting devices are not available (Canham 1993). The lack of such devices makes the fabrication of silicon-based optoelectronic integrated circuits not suitable. The

possible solution to this problem is the formation of new silicon structural forms with nanoscale crystallites, wires, and dots. As the dimensions become less than 6–7 nm, quantum–mechanical effects start to act in such way that luminescence efficiency increases (Canham 1990). Another possible solution is to use compound semiconductor materials that possess a direct band gap such as gallium arsenide, gallium nitride, and zinc oxide.

Zinc oxide is wide direct band gap semiconductor (Eg = 3.35 eV) with a high photoluminescence efficiency, low bond energy of excitons (60 meV) and high transmittance in the optical range (90%). ZnO nanorod ensembles showed internal quantum efficiency of 75 and 33%, respectively, at 125 and 300 K (Al-Suleiman et al. 2009). Recently, zinc oxide materials gained considerable attention, due to the existence of mature fabrication technologies.

Light-emitting devices, laser diodes, surface acoustic wave devices, different sensors, and piezoelectric devices may be based on zinc oxide material (Ozgur et al. 2005; Wang 2004). At present time single-crystal zinc oxide wafers are already available, but their size is small (not more than 3 inches) and their cost is very high (up to 3500 USD) (Dem'yanets and Lyutin 2008; Ehrentraut et al. 2006). It is no wonder that devices based on such wafers are still a long way to reach the commercial production. It is important to note that, while the technology for fabricating zinc oxide wafers is well developed, the production of large single-crystal zinc oxide wafers is not expected in the nearest future. Therefore, developing technologies for zinc oxide deposition as films on large silicon wafers seem to be promising. ZnO/Si structures offer the possibility, within conventional microelectronic technology, to fabricate devices based on zinc oxide. Such approach offers a new way of integration with the opportunity to produce new integrated devices combining silicon-based electronic ICs and zinc oxide-based devices. The formation of zinc oxide films on the surface of monocrystal silicon presents the problems typical of the heterostructure technologies as silicon and zinc oxide have different crystal lattice and thermo-mechanical behavior. Zinc oxide has hexagonal lattice of wurtzite type with $a_o = 0.324$ nm and $c_o = 0.521$ nm lattice constant and coefficients of thermal expansion of 6.51 and 3.02 μm m^{-1} K^{-1} (Albertsson et al. 1989). Silicon has cubic lattice with lattice constant $a_o = 0.53$ nm and coefficient of thermal expansion of 2.6 μm m^{-1} K^{-1} (Okada and Tokumaru 1984). The differences in crystal lattice types and lattice constants result in the evolution of mismatch stress at the silicon and the deposited zinc oxide film interface. The difference in thermal expansion coefficients results in thermal stress. Mismatch and thermal stresses cause elastic deformations that in turn cause plastic deformations. Since the thickness of the zinc oxide film deposited is always less than the thickness of the silicon substrate, damaging defect arise predominantly in the ZnO film causing cracks. A radical solution for such problem is to introduce a buffer layer between the zinc oxide film and the silicon wafer. Porous silicon formed by anodic etching of silicon in hydrofluoric acid is one possible way to form the buffer layer. Porous silicon (e.g., nano/micro-porous, meso-porous, and macro-porous) layers from tens of nanometers to tens of micrometers in thickness may be obtained by varying the regimes of the anodic etching (e.g., the anodic current density), electrolyte composition, and doping level of the mono-crystal silicon under anodization. The pioneer work on using PS as a buffer layer for the formation of silicon heterostructures (i.e., PbS/Si) using chemical vapor deposition (CVD) method was published in 1994 (Bondarenko et al. 1994). In a subsequent study, the buffer layer approach was used for the successful deposition of GaAs and diamond films (Raiko et al. 1996) on silicon by the CVD method. In both studies, was shown that the mandatory requirement for the success of such approach is to fill mesoscopic pore channels with the same material of the film that will be grown on top of the surface. Once the pores are filled, the film can be grown up to needed thickness. The beneficial effect of the buffer PS layer on the structure of the deposited films has been reported in several studied for PbS, PbTe, ZnSe, and CdSe (Levchenko et al. 1999; Yakovtseva et al. 2000; Chubenko et al. 2009a, b).

All the above mentioned studies on the use of the PS buffer layer for the heteroepitaxial structure formation including zinc oxide deposition deal with so-called dry deposition processes, namely molecular beam epitaxy (MBE) and CVD methods which are conducted at relatively high temperatures. Such processes are not suitable for the integration of zinc oxide device onto silicon wafer. Deposition of zinc

oxide layers should be carried out in the final stages of IC fabrication to avoid the formation of stress-induced defects in the zinc oxide layer due to the IC processing steps at temperature between 500 and 850 °C. In this approach, zinc oxide should be deposited at low temperatures to not damage active regions of silicon ICs already formed. The low-temperature deposition of zinc oxide films may be made by either the electrochemical deposition or hydrothermal synthesis from the solutions of zinc salts heated to 70–90 °C. By the liquid methods mentioned zinc oxide can be obtained in various structural forms (Cembrero and Busquets-Mataix 2009; Lincot 2005). The basic forms are shown schematically in Fig. 1. The hydrothermal method can provide arrays of ZnO crystals from several nanometers to micrometers in size. The potentiality of the electrochemical deposition is more comprehensive. Varying the parameters of the electrochemical deposition process (i.e., either current density or voltage) zinc oxide may be obtained both in the form of single crystals (as in the case of the hydrothermal method) and in the form of continuous polycrystalline and, in certain conditions, epitaxial films (Baruah and Dutta 2009a, b).

As for the electrochemical deposition of zinc oxide into PS, to authors' knowledge only a few articles were published (Liu et al. 2002, 2003). However, these studies do not show features of the deposition process and the structure of zinc oxide in the pore channels and at the surface as well as do not include any practical recommendations.

In this study, the features of the electrochemical deposition of zinc oxide into pore channels and on the surface of the PS layers, the structure and luminescent properties of zinc oxide films are reported, possible ways for the improvement of optical properties of the films and possible fields of application are discussed.

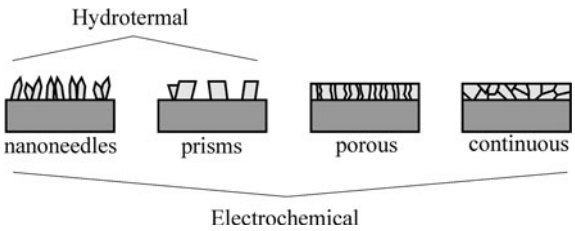

Fig. 1 Variety of ZnO morphological structures provided by wet deposition techniques: electrochemical and hydrothermal methods

Experimental

The electrochemical deposition of ZnO was carried out at 95 °C from non-aqueous solutions based on dimethyl sulfoxide (DMSO) containing 0.03 M of zinc chloride $ZnCl_2$ and 0.1 M of potassium chloride to ensure good conductivity. Only analytical grade quality components were used to prepare the solutions. Electrochemical deposition of ZnO was performed on n^+-type antimony-doped Si (111) substrates (0.01 Ω cm) with PS buffer layers which were prepared by anodizing silicon substrates in the $HF:H_2O:C_3H_7OH = 1:3:1$ solution at the current density 70 mA/cm^2 for different times. Porosity of the PS was 65%. The electrochemical deposition of ZnO onto PS electrodes was studied by cyclic voltammetry. A three-electrode glass electrochemical cell equipped with a magnetic stirrer and a temperature control unit was used. A standard commercial Ag/AgCl electrode served as the reference electrode. The counter electrode was a platinum wire. PS electrodes were prepared as described above for PS substrates for the ZnO deposition. Before experiments the native SiO_2 layer was removed in 4.5% HF solution and PS were thoroughly cleaned from HF with deionized water jet. Reproducibility of the PS electrodes was controlled by checking the equilibrium potential in the electrochemical bath.

The deposition of zinc oxide from the non-aqueous solution was made in the galvanostatic regime at a cathodic current density of 0.5 mA/cm^2. Deposition time in all cases was 20 min.

All the electrochemical experiments were performed with the PI-50-1.1 analog potentio-galvanostat controlled by a computer via Advantech PCI-1710HG analog-to-digital converter.

In addition to the electrochemical growth of the zinc oxide film on the PS surface, zinc oxide nanocrystals were also deposited thereafter. This was made using hydrothermal synthesis method. The hydrothermal synthesis of ZnO crystals was carried out from the 0.1 M equimolar aqueous solution of zinc nitride $Zn(NO_3)_2$ and hexamethylenetetramine $C_6H_{12}N_4$. The pH of the solution was adjusted to 5 by adding some quantity of ZnO (Baruah and Dutta

2009a, b). $C_6H_{12}N_4$ was added just before the experiments. The reaction chamber volume was 20 mL. Thermo control unit was used to maintain the temperature of the chamber. Substrates were immersed into the solution using a Teflon holder and then the reaction chamber was heated up to the target temperature. After a certain time (i.e., 3 h) of deposition, substrates were rinsed in deionized water and dried out on the air (Ashfold et al. 2007; Liu et al. 2006). The surface morphology and composition of ZnO films and ZnO crystals deposited were studied by the Hitachi S-4800 scanning electron microscope (SEM) operating at 15 kV. The phase constitution was studied by the X-ray diffractometry (XRD) technique using the CuKα source. The photoluminescence spectra of ZnO were measured at room temperature by monochromator with a Xe lamp (1000 W) as an excitation light source and Hamamatsu S7031 FFT-CCD image sensor as a detector. To cut out monochromatic lines from a Xe lamp spectrum, another monochromator was used.

Results and discussions

Electrochemical deposition of ZnO from non-aqueous solution

The main problem that should be solved for the zinc oxide deposition into pore channels of PS is how to carry out the electrochemical process (i.e., electrolyte composition, potentials, and current densities of the process) to prevent PS itself from etching and oxidation when it is submerged into the electrolyte. Due to a high effective internal area (e.g., for mesoPS it is equal to 200–600 m^2/cm^3 (Herino 1997)) PS displays extremely high chemical activity in many liquid mediums where monocrystal (nonporous) silicon remains inert. As an example, PS, although slowly, is etched in hot water (i.e., 75–85 °C (Li et al. 1992)). Monocrystal silicon nearly does not react with diluted alkalis solutions, while the PS etching in such solution flows very actively with hydrogen evolution and such reactivity of PS makes impossible to deposit zinc oxide electrochemical from aqueous solutions of zinc salts heated to 70–80 °C. Only non-aqueous solutions are suitable. Figure 2 shows cyclic voltammograms of the PS electrode in the non-aqueous DMSO solution containing various

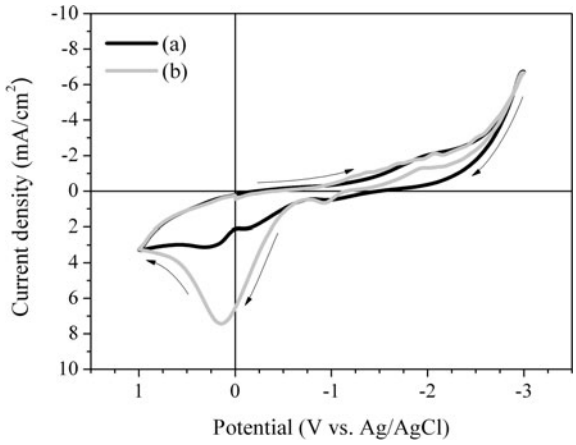

Fig. 2 Cyclic voltammograms of the PS electrode in the non-aqueous DMSO solution containing: (*a*) 0.03 M $ZnCl_2$, 0.1 M KCl and (*b*) 0.06 M $ZnCl_2$, 0.1 M KCl at 80 °C. The scan rate is 1 V/s

concentrations of zinc chloride (0.03 M and 0.06 M $ZnCl_2$) at 80 °C. A change in the concentration of zinc ions resulted only in an intensification of the dissolution peak in the anodic branch of the voltammogram in the range of 0.2 V, suggesting that this peak is related with the oxidation of zinc ions. At the cathode polarization, only a current plateau in the range from −1.8 to −2.4 V is observed to be associated with the zinc oxide deposition. Current densities for electrochemical deposition of zinc oxide in galvanostatic regime were evaluated by current measurements during deposition in a potentiostatic regime.

Zinc oxide was deposited on silicon wafers with PS layers of various thicknesses formed on the front side of the wafers. Samples were named as A, B, and C. The thicknesses of the PS layers were 1 μm for the sample A, 3 μm for the sample B, and 6 μm for the sample C. These thicknesses were provided by anodizing silicon wafers for 20 s, 1 min, and 2 min, respectively. The SEM study showed that a mean diameter of pore channels is 20 nm, a mean distance between centers of neighboring pores is 50 nm, and wall thickness of the silicon skeleton is 30 nm. In accordance with the international classification of porous bodies, such PS is related to meso-porous material.

The electrochemical deposition of any material into PS is a specific challenge. The matter is that elements of the silicon skeleton remaining between the pore channels represent a thin columns with

30 nm in thickness and 1–6 μm in length with an aspect ratio greater than 1:100. When PS is placed into liquid electrolyte, a space charge layer is generated in the silicon skeleton. Depending on the thickness and other conditions, elements of the silicon skeleton become partially or completely depleted of charge carriers, locally reducing the electrically conductibility of the material. It means that if the thickness of PS is low silicon crystallites forming PS skeleton have good conductivity and electrochemical deposition of any material will take place mainly on top of the PS layer, and vice versa, when PS layer has high thickness deposition will take place at the bottom part of the PS pores.

Figure 3a shows a general SEM pattern of the cross-section of the sample A. Figure 3b and c show cross-section views of this sample at the ZnO and PS interface and at the bottom regions of the PS layer correspondingly. Figure 3d illustrates a plane view of the sample. As seen from Fig. 3a, a zinc oxide layer is observed on the PS surface that drastically differs from the PS structure. The thickness of this zinc oxide layer is equal to 480 nm, the layer surface is uneven, and the layer consists of very small grains. X-ray microanalysis showed that this layer contains 50 at.% of zinc and 50 at.% of oxygen (i.e., stoichiometric zinc oxide). As seen from Fig. 3b, the zinc oxide layer refers to glass-like amorphous material partially penetrating into the pore channels of PS down to a depth of about 100–200 nm. Referring to Fig. 3a and c, single separated zinc oxide nano particles 10–15 nm in size are observed on the pore sidewalls deeper in the PS layer down to the bottom of the PS layer. So, for the sample A with 1 μm thick PS layer, zinc oxide penetrates into whole depth of the pores, however it fills the PS layer only partially, not completely. Nevertheless, as evident from the sample cross-section, the zinc oxide layer

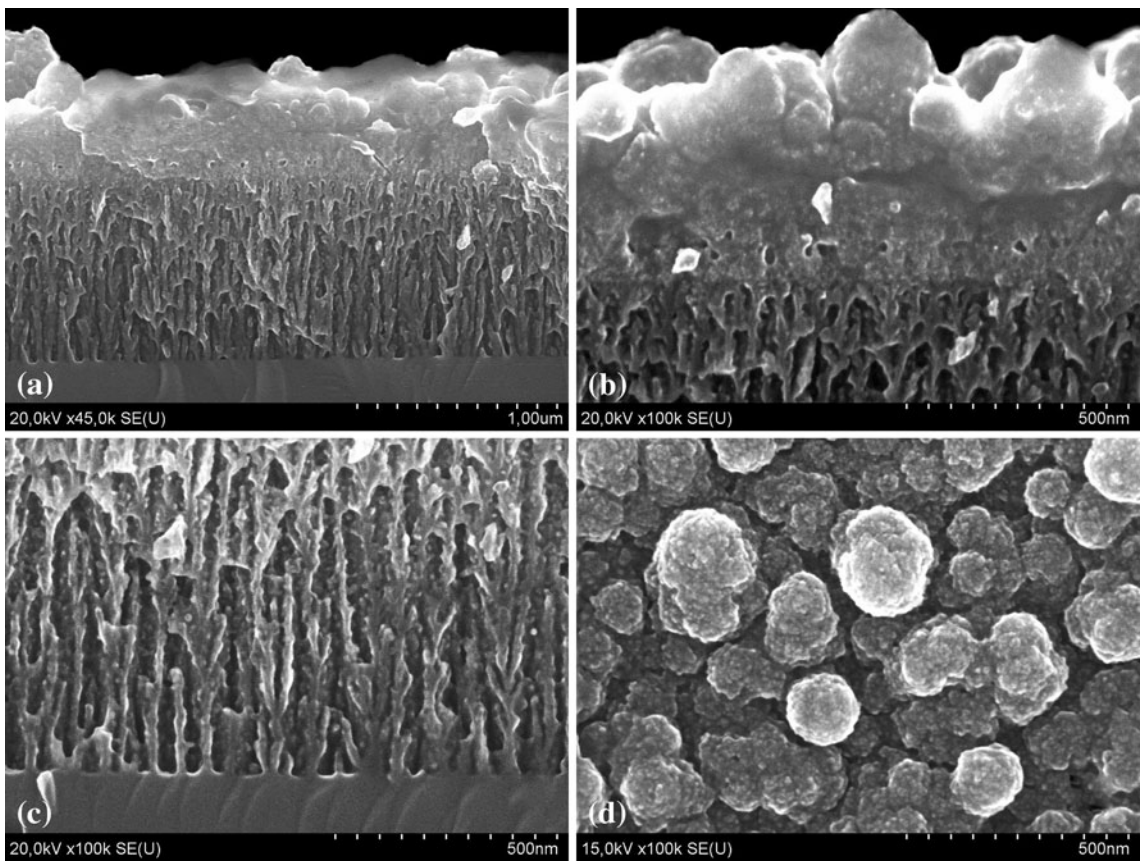

Fig. 3 SEM image of the sample A after ZnO deposition from DMSO solution representing (**a**) cross-section full view, (**b**) interface between deposited ZnO and porous silicon, (**c**) bottom part of the porous silicon, and top view (**d**)

deposited on the surface seems to be continuous. As for the surface analysis of the sample A, the zinc oxide layer consists of round aggregates mainly 150–200 nm in diameter as shown in Fig. 3d. Some larger aggregates 300–400 nm in size are observed as well. The SEM photograph also shows that aggregates in turn consist of a great number of nano particles only a few nanometers in size.

Figure 4a shows a general SEM pattern of the cross-section of the sample B. Figure 4b and c show cross-section view of this sample at ZnO/PS interface and at the bottom regions of the PS layer correspondingly. Figure 4d illustrates a plane view of the sample.

As can be seen in Fig. 4a and b, the zinc oxide layer is observed at the PS surface. The thickness of this layer is about 200 nm. X-ray microanalysis showed that this layer also contains 50 at.% of zinc and 50 at.% of oxygen as in the sample A. Sample B is characterized by much deeper filling of pore channels with zinc oxide as indicated in Fig. 4a and c. Nano particles of zinc oxide in sufficiently large quantity are observed on the pore sidewalls throughout the whole 3 μm thickness of the PS layer, including pore bottoms at the interface with the mono-crystal silicon substrate. These zinc oxide nano particles are sized from 20–25 to 40–50 nm. Referring to Fig. 4d, the analysis of the SEM images of the sample B surface shows that the zinc oxide layer deposited on the surface consists of round aggregates of 200–400 nm in diameter like it is also in the surface layer of sample A. As compared with sample A, sample B presents more uniform zinc oxide layer containing less large aggregates. As seen from Fig. 4d, aggregates in turn consist of a great number of fine nano particles of 15–25 nm in size.

Figure 5a–d show SEM images of the sample C. Referring to Fig. 5a, the zinc oxide film thickness on

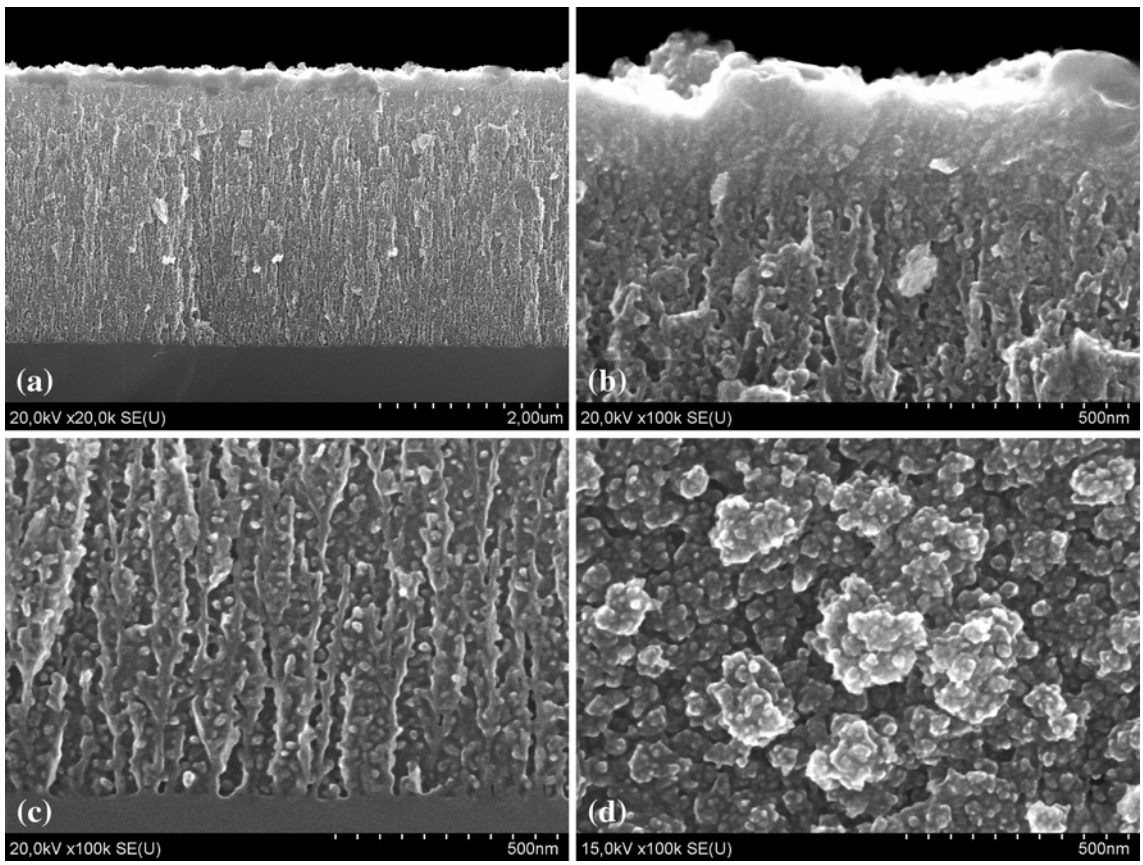

Fig. 4 SEM image of the sample B after ZnO deposition from DMSO solution representing (**a**) cross-section full view, (**b**) interface between deposited ZnO and porous silicon, (**c**) bottom part of the porous silicon, and top view (**d**)

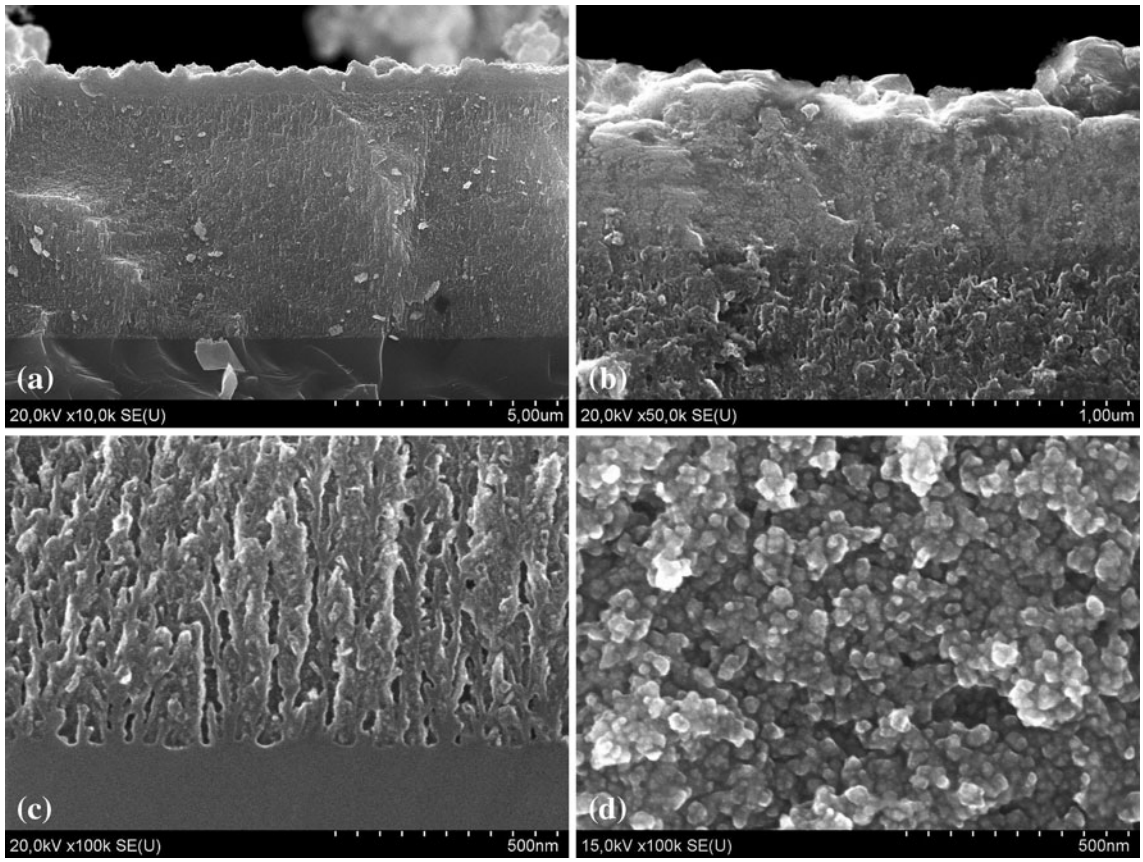

Fig. 5 SEM image of the sample C after ZnO deposition from DMSO solution representing (**a**) cross-section full view, (**b**) interface between deposited ZnO and porous silicon, (**c**) bottom part of the porous silicon, and top view (**d**)

the surface is about 700 nm. Zinc oxide fills the whole 6 μm thick PS layer. Zinc oxide inside pores looks like homogeneous glass-like material though single separated nano particles up to 70–80 nm in size are observed. The pore channels are filled with zinc oxide though, not completely. The structure of the pore channels, characteristic of the initial mesoPS, is observed in the sample C, despite of pore filling with zinc oxide. The analysis of the SEM plan view images showed that the surface of zinc oxide layer consists of aggregates constituted by zinc oxide nano particles. Diameter of nano particles is 20–50 nm to be 2–3 times greater than for the sample B.

The results of the experiments show that zinc oxide can be deposited on the substrates with PS buffer layer from non-aqueous electrolytes based on DMSO and zinc chloride. In this case the thickness of the PS layer, i.e., the height of silicon crystallites making up the skeleton of PS, is of considerable importance for the pore filling with zinc oxide. The effective pore filling for the PS type used was achieved only with the PS layer thickness not less than 5 μm. Furthermore, when material penetrates deeply into the porous matrix, its adhesion to the substrate surface increases.

Hydrothermal synthesis of ZnO crystals

The hydrothermal deposition technique is an easy method for the formation of zinc oxide nano crystals on any substrate, including dielectric ones, of any area. Crystals obtained by this technique are noted for the high crystal perfection. This is one of the factors that allows manufacturing not only arrays of nano and microcrystals, but ingots of large diameter for the ZnO substrates production as well.

In this study, the deposition of zinc oxide crystals on the surfaces of the samples A, B, and C was made

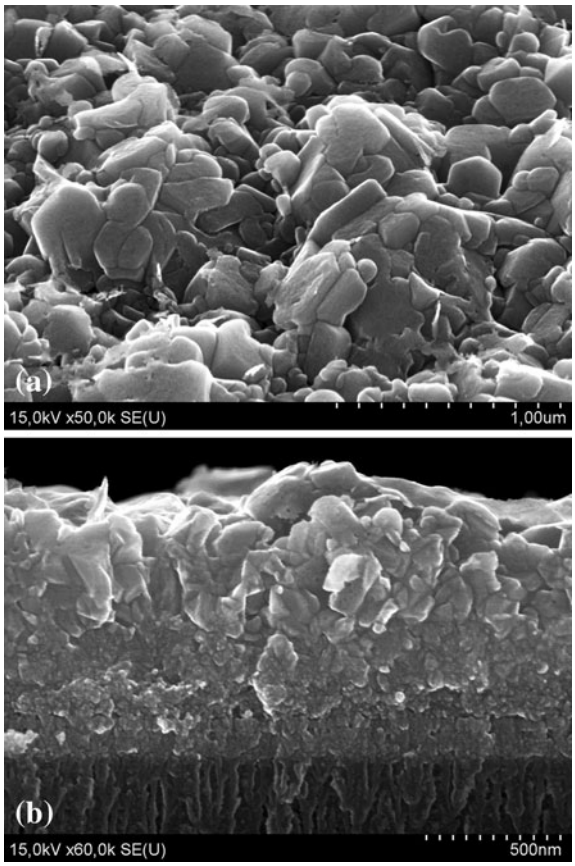

Fig. 6 SEM image of the sample A after hydrothermal ZnO deposition representing the top view (**a**) and cross-section (**b**)

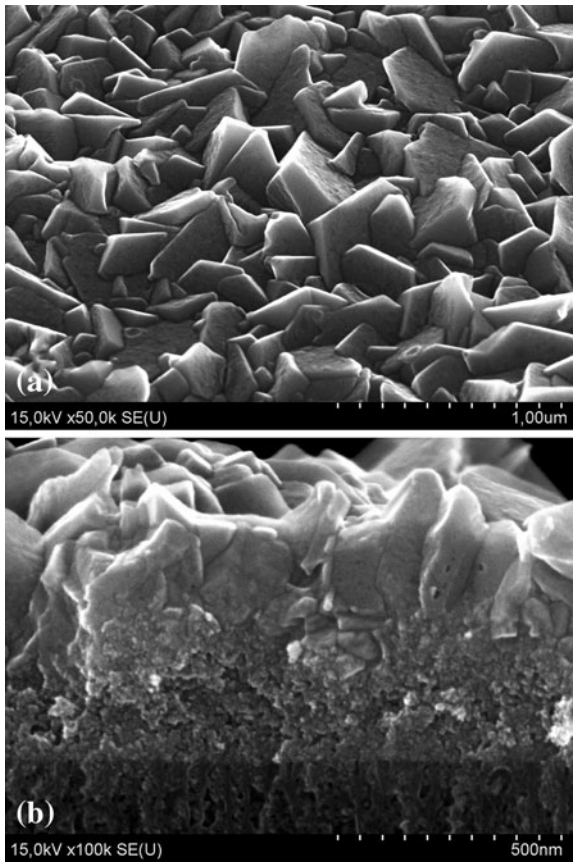

Fig. 7 SEM image of the sample B after hydrothermal ZnO deposition representing the top view (**a**) and cross-section (**b**)

to provide ultraviolet luminescence characteristics of the zinc oxide layer formed on the buffer PS layer.

Figure 6a shows plan view SEM image of the sample A after the hydrothermal treatment. It is evident that the film consisted of hexahedral crystals characteristic of zinc oxide crystals having the hexagonal lattice formed on the sample surface. The film surface contains a lot of structural defects. The SEM image of the sample cross-section shown in Fig. 6b consists of random crystals on top of the surface of the zinc oxide electrochemically deposited. The thickness of the hydrothermal ZnO is 500 nm. The clear interface between the electrochemical and hydrothermal layers of zinc oxide is not observed. Noteworthy also is the smooth zinc oxide/porous silicon junction without a sharp boundary and cross cracks.

Figure 7a shows plan view SEM images of the sample B after the hydrothermal treatment. In contrast to the sample A, zinc oxide film on the surface of the sample B consists of grown together hexahedral crystals having well-defined faces. The size of single crystals is 100–300 nm. The SEM image of the sample cross-section shown in Fig. 7b displays that crystals of the hydrothermal zinc oxide are all-of-a-piece as distinct from the sample A and grow directly on the zinc oxide layer electrochemically deposited. The layer thickness is approximately 500 nm.

Figure 8 shows SEM plan and cross-sectional images of the sample C. As seen from Fig. 8a and b, for the sample C the situation is similar to sample B, however, the crystals are larger in size and they separated from one another more distinctly. Crystals are up to 600 nm in diameter. They settle at a big angle to the sample surface that relates to the developed surface morphology of the initial substrate.

It may be concluded that the size and arrangement of zinc oxide crystals deposited by the hydrothermal

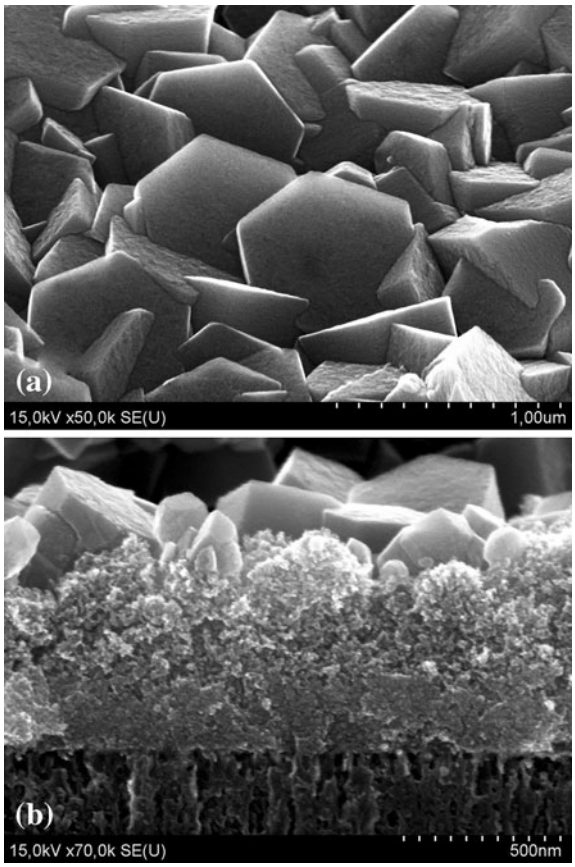

Fig. 8 SEM image of the sample C after hydrothermal ZnO deposition representing the top view (**a**) and cross-section (**b**)

method considerably depend on the surface morphology of the initial substrate, i.e., the surface of the zinc oxide film electrochemically deposited, which in turn is conditioned by the characteristics of the buffer PS layer.

XRD analysis

X-ray diffraction analysis was made only for the samples A and C since an inherent difference between the samples B and C was not revealed by the study on the surface morphology. Figure 9 shows XRD patterns for the samples A and C before and after the zinc oxide hydrothermal deposition. Peaks associated with the silicon substrate of (111) crystallographic orientation are well observed in all XRD patterns. Only one peak associated with zinc oxide crystals corresponding to $(11\tilde{2}1)$ and $(10\tilde{1}2)$ phases is seen in the XRD patterns before the hydrothermal

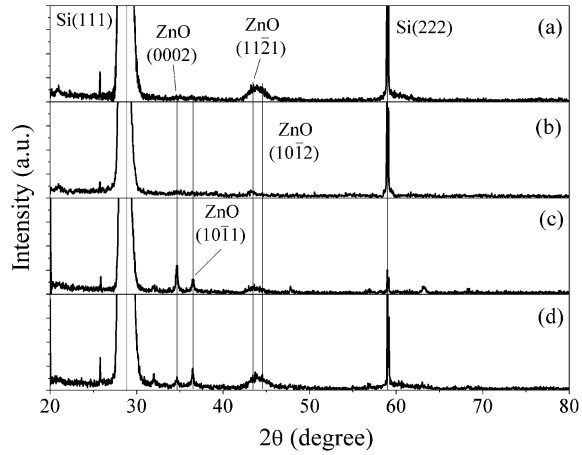

Fig. 9 XRD patterns of the samples A and C before (*a*), (*b*) and after (*c*), (*d*) hydrothermal ZnO deposition. *Source*: CuKα

deposition. We suppose that this peak consists of two peaks. Presumably these neighboring peaks join into one wide band indicating the presence of amorphous zinc oxide. On the whole, the zinc oxide film obtained may be described as structured microcrystalline film. After the zinc oxide crystal deposition by the hydrothermal method, peaks corresponding to (0002) and $(10\tilde{1}1)$ phases of zinc oxide appear in the XRD patterns. The ratio of peaks for the samples A and B is different to be once more indicative of the difference in the structure of these samples.

Photoluminescence properties

Analysis of the photoluminescence of semiconductor materials is a powerful tool to obtain information about the structure of energy bands and crystal perfection. Photoluminescence spectra reveal the presence of impurities and lattice defects that result in the formation of impurity levels in the band gap, which, in turn, decrease the intensity of exciton luminescence bands and give new proper luminescence bands.

Figure 10 shows the photoluminescence spectra of the zinc oxide films electrochemically deposited on the silicon substrates with the PS buffer layer from the non-aqueous solution and zinc chloride. As seen from Fig. 10, zinc oxide films demonstrate only one wide photoluminescence band with maximum at near 510–550 nm in the yellow range of the

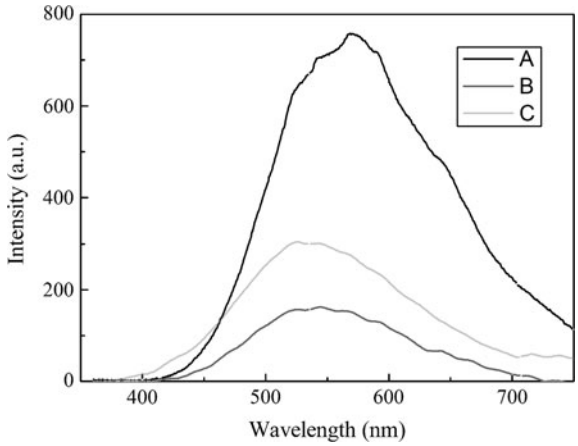

Fig. 10 Photoluminescence spectra of samples *A*, *B*, and *C* directly after ZnO deposition from DMSO solution

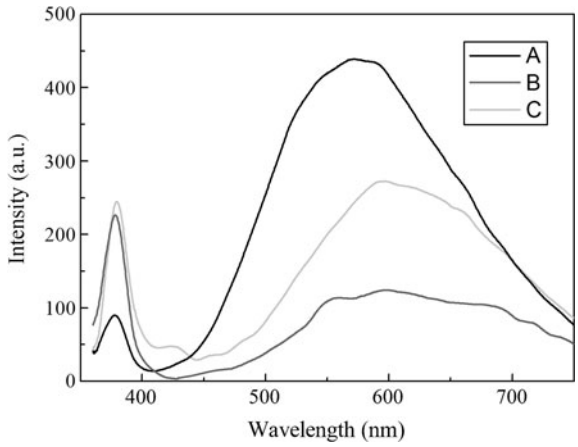

Fig. 11 Photoluminescence spectra of samples *A*, *B*, and *C* directly after ZnO hydrothermal deposition

electromagnetic radiation spectrum. As the samples under study were not doped specially and were free from unintentional impurities, it is obvious that this band is conditioned by internal defects of material. As seen in Fig. 11, photoluminescence spectra drastically changed after the deposition of zinc oxide crystals on the surfaces of the zinc oxide layers electrochemically deposited. Every sample gained extra photoluminescence band with maximum in the range of short-wave ultraviolet at the wavelength of 375 nm. This wavelength corresponds to the band gap energy of perfect ZnO crystals (Eg = 3.35 eV) and is emitted due to the recombination of free excitons. Maximum of the band in the yellow spectral region was shifted to the wavelength

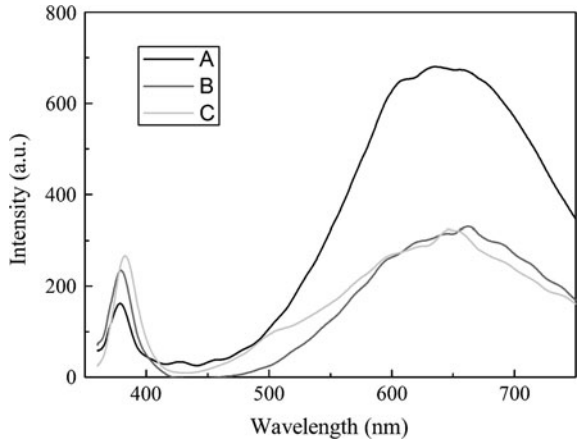

Fig. 12 Photoluminescence spectra of samples *A*, *B*, and *C* directly after ZnO hydrothermal deposition annealed at 400 °C for 30 min in air

580–600 nm. Noteworthy also is a correlation of the intensities of the photoluminescence bands from ultraviolet and yellow spectral regions. The more intensive is the yellow band (sample A), the less intensive is the ultraviolet band and vice versa. As shown in SEM images, the film of zinc oxide crystals deposited by hydrothermal method on the sample A has more structural defects as well as more lattice defects. Thermal annealing in air at temperature of 400 °C for 30 min resulted in both further shift of maxima of defect luminescence into the red spectral region and the intensity change as shown in Fig. 12.

The photoluminescence band observed in the yellow range may consist of two independent bands conditioned by the recombination processes via the levels in the semiconductor band gap due to ionized oxygen vacancies and oxygen atoms in the interstitial sites of the ZnO crystal lattice (Zhang et al. 2008). The photoluminescence band emitted by the oxygen vacancies has maximum in the more short-wave (500–550 nm) range of the spectrum, while the band emitted by the oxygen atoms in the interstitial sites has maximum at longer (650 nm) wavelength. The positions and intensities of maxima can vary depending on wavelength of the exciting radiation (Zhang et al. 2008) and material structure (Zhang et al. 2008; Mo et al. 1998).

When the ZnO film is heated in water or annealed in air, free oxygen is adsorbed by the material surface, ionized, and embedded in the ZnO crystal

lattice. Hence, the most part of the oxygen vacancies is compensated, while the concentration of the oxygen atoms in the interstitial sites remains the same and even increases at the surface. These processes result in the decrease in the intensity of the photoluminescence band (at 500–550 nm) associated with the ionized oxygen vacancies. The intensity of the photoluminescence band conditioned by the oxygen atoms in the interstitial sites of the ZnO crystal lattice remains the same at that or may slightly increase (Zhang et al. 2008).

Applications and aspects of integration with the silicon technology

The main advantage of liquid methods for the zinc oxide production is the low outlay for the manufacturing equipment and the low price of the production process. These methods are suitable for the fabrication of low-cost photovoltaic devices and sensors. Films and crystals formed by the electrochemical method contain lots of structural defects and using it as active regions in light-emitting devices is not advantageous. However, these films are well suitable as transparent conducting electrode for solar cells, photodetectors, and light-emitting devices. High-temperature oxidation enhances properties of the zinc oxide films and expands possible fields of application. However, these films are inferior to MBE and CVD films in quality.

Figure 13a illustrates the construction of a silicon photodetector with a transparent conducting electrode made of electrochemically deposited zinc oxide, and Fig. 3b shows the measured spectral sensitivity of the device. The photodetector consists of p-type silicon substrate with the PS layer at the surface. The structure is conformally filled with zinc oxide which forms a continuous surface film. The spectral sensitivity broadening in the long-wave range of the electromagnetic spectrum at the energy lower than silicon band gap energy is due to the presence of levels in the band gap caused by surface defects in the PS layer.

Porous zinc oxide films electrochemically formed inside PS were also used as chemical gas sensors to detect hydrogen and gaseous hydrocarbons (Basu and Basu 2009) as piezoelectric devices (Ozgur et al. 2005). The high-quality zinc oxide nano crystals formed by the hydrothermal method was used to build light-emitting devices and nano-scaled piezoelectric energy generator (Wang 2008).

The use of silicon substrates opens up the possibility to use commercial industrial technological equipment for the large substrates assuring the reduction of manufacturing cost of devices based on zinc oxide. Devices based on zinc oxide deposited on silicon substrate can be made not only in discrete form but also integrated with conventional silicon integrated circuits either in the same package by hybrid technology or in the same chip.

When zinc oxide base devices are integrated in silicon ICs within the same chip, a treatment of silicon wafer with zinc oxide regions already formed became a considerable problem. Despite of buffer layers employed, the risk of the zinc oxide layer damage during high-temperature epitaxial and diffusion processes is very high. So, the zinc oxide deposition can be done after the formation of the active regions of silicon electronic devices and, as an example, before the formation of the IC metal layers, seems to be more advantageous. The low process temperature (<100 °C) of the liquid methods of the zinc oxide deposition eliminates the risk of any kind of damage for the p–n junctions already formed in the silicon substrate. Zinc oxide may be

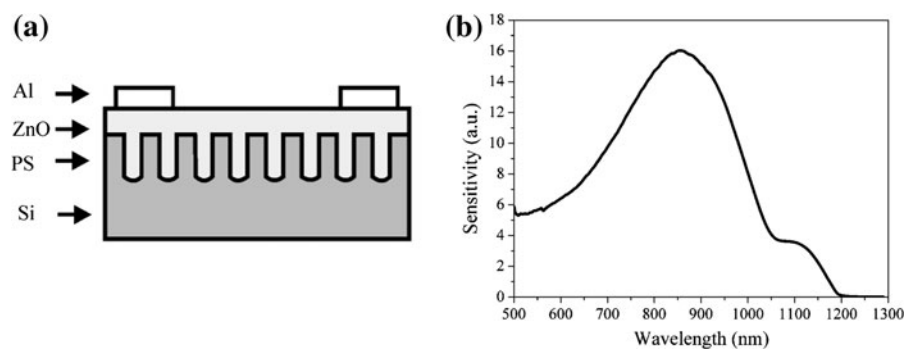

Fig. 13 **a** Construction and (**b**) spectral sensitivity of photodetector based on the Si/PS/ZnO heterojunction

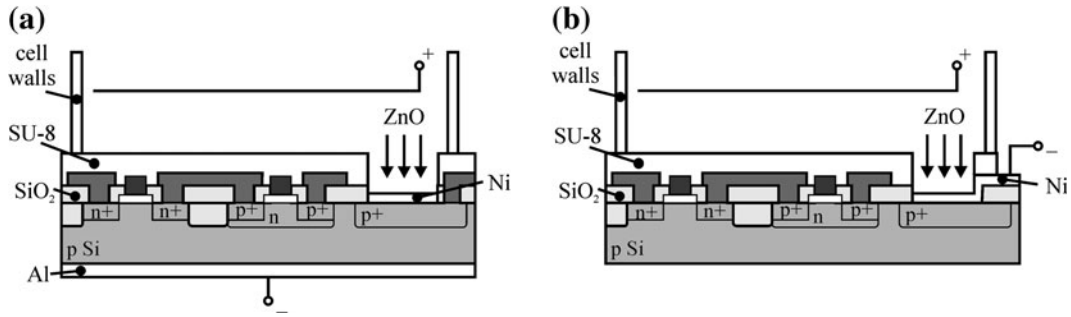

Fig. 14 Variants of the ZnO electrochemical deposition on silicon substrates with already formed integrated circuits: (**a**) contact from the backside of the Si substrate and (**b**) contact from the top side

deposited locally into the exposed regions of the masking layer. When the electrochemical deposition is used, an electric contact may be provided either from back side or front side of the substrate as illustrated in Fig. 14. For the first case, an ohmic contact should be provided to the back side of the substrate, and for the second case, special contact pads should be created on the front side. The hydrothermal method does not need any electric contact but a strictly local zinc oxide deposition cannot be done by such method. The ZnO in excess may be removed at further etching of the masking layer (e.g., lift-off process).

Conclusions

This study shows that zinc oxide can be deposited from non-aqueous electrolytes based on DMSO and zinc chloride on the surface of a buffer mesoporous layer. Depending on the thickness of the buffer layer, zinc oxide can be deposited either on the surface only or into the pores and on the surface simultaneously. The full pore filling start to take place as the thicknesses of the PS layer reaches 5 μm. Material deposited is microstructured zinc oxide of a stoichiometric composition. The layer of perfect zinc oxide crystals formed by the hydrothermal method on the surface of the electrochemically deposited zinc oxide improved optical characteristics of the whole structure. The structure obtained demonstrated two photoluminescence bands with maxima in ultraviolet and yellow spectral regions. The new technique presented proves that the possibility to integrate within a chip zinc oxide devices with silicon-based devices is on the way.

Acknowledgments The study has been supported by Belarus Government Research Program "Nanomaterials and nanotechnologies", grant 6.12.03 and by the Italian company Rise Technology S.r.l. Authors would like to thank V. Tzibulsky from "Belmicrosystems" (Minsk, Belarus) for help in SEM images preparation, A. Puskarev, L. Postnova and V. Levchenko from "Scientific-Practical Materials Research Centre of NAS of Belarus" SSPA for their help in XRD investigations, and V. Yakovtseva and R. Crescenzi respectively from Belarusian State University of Informatics and Radioelectronics and University of Rome "La Sapienza", Electronic Department for the fruitful discussion, and also O. Kozlova and A. Yermalovich for their help in experiments implementation.

References

Albertsson J, Abrahams SC, Kvick A (1989) Atomic displacement, anharmonic thermal vibration, expansivity and pyroelectric coefficient thermal dependences in ZnO. Acta Cryst B45:34–40. doi:10.1107/S0108768188010109

Al-Suleiman MAM, Bakin A, Waag A (2009) Mechanisms for high internal quantum efficiency of ZnO nanordos. J Appl Phys 106:063111

Ashfold MNR, Doherty RP, Ndifor-Angwafor NG, Riley DJ, Sun Y (2007) The kinetics of the hydrothermal growth of ZnO nanostructures. Thin Solid Films 515:8679–8683. doi:10.1016/j.tsf.2007.03.122

Baruah S, Dutta J (2009a) Hydrothermal growth of ZnO nanostructures. Sci Technol Adv Mater 10:013001–013019. doi:10.1088/1468-6996/10/1/013001

Baruah S, Dutta J (2009b) pH-dependent growth of zinc oxide nanorods. J Cryst Growth 311:2549–2554. doi:10.1016/j.jcrysgro.2009.01.135

Basu S, Basu PK (2009) Nanocrystalline metal oxides for methane sensors: role of noble metals. J Sens 2009:861968–861988. doi:10.1155/2009/861968

Bondarenko V, Vorozov N, Dikareva V, Dorofeev A, Levchenko V (1994) Heteroepitaxial growth of lead sulfide on silicon. Tech Phys Lett 20:410–411

Canham LT (1990) Silicon quantum array fabrication by electrochemical and chemical dissolution of wafers. Appl Phys Lett 57:1046–1048. doi:10.1063/1.103561

Canham LT (1993) Progress toward crystalline-silicon-based light-emitting diodes. MRS Bull 18:22–28

Cembrero J, Busquets-Mataix D (2009) ZnO crystals obtained by electrodeposition: statistical analysis of most important process variables. Thin Solid Films 517:2859–2864. doi:10.1016/j.tsf.2008.10.069

Chubenko E, Bondarenko V, Balucani M (2009a) Visible photoluminescence of zinc oxide films electrochemically deposited on silicon substrates. Tech Phys Lett 35:1160–1162

Chubenko E, Klyshko A, Petrovich V, Bondarenko V (2009b) Electrochemical deposition of zinc selenide and cadmium selenide onto porous silicon from aqueous acidic solutions. Thin Solid Films 517:5981–5987. doi:10.1016/j.tsf.2009.03.134

Dem'yanets LN, Lyutin VI (2008) Status of hydrothermal growth of bulk ZnO: latest issues and advantages. J Cryst Growth 310:993–999. doi:10.1016/j.jcrysgro.2007.11.145

Ehrentraut D, Sato H, Kagamitani Y, Sato H, Yoshikawa A, Fukuda T (2006) Solvothermal growth of ZnO. Prog Cryst Growth Charact Mater 52:280–335. doi:10.1016/j.pcrysgrow.2006.09.002

Herino R (1997) Pore size distribution in porous silicon. EMIS Datarev Ser 18:89–96

ITRS (2009) International technology roadmap for semiconductors. http://www.itrs.net/Links/2009ITRS/Home2009.htm

Levchenko V, Postnova L, Bondarenko V, Vorozov N, Yakovtseva V, Dolgyi L (1999) Heteroepitaxy of PbS on porous silicon. Thin Solid Films 348:141–144. doi:1016/S0040-6090(99)00052-8

Li KH, Tsai C, Shih S, Hsu T, Kwong DL, Campbell JC (1992) The photoluminescence spectra of porous silicon boiled in water. J Appl Phys 72:3816–3818. doi:10.1063/1.352280

Lincot D (2005) Electrodeposition of semiconductors. Thin Solid Films 487:40–48. doi:10.1016/j.tsf.2005.01.032

Liu YL, Liu YC, Liu YX, Shen DZ, Lu YM, Zhang JY, Fan XW (2002) Structural and optical properties of nanocrystalline ZnO films grown by cathodic electrodeposition on Si substrates. Phys B 322:31–36. doi:10.1016/S0921-4526(02)00594-X

Liu YL, Liu YC, Yang H, Wang WB, Ma JG, Zhang JY, Lu YM, Shen DZ, Fan XW (2003) The optical properties of ZnO filmsgrown on porous Si templates. J Phys D Appl Phys 36:2705–2708. doi:10.1088/0022-3727/36/21/017

Liu Ch, Masuda Y, Wu Y, Takai O (2006) A simple route for growing thin films of uniform ZnO nanorod arrays on functionalized Si surfaces. Thin Solid Films 503:110–114. doi:10.1016/j.tsf.2005.12.075

Mo CM, Li YH, Liu YS, Zhang Y, Zhang LD (1998) Enhancement effect of photoluminescence in assemblies of nano-ZnO particles/silica aerogels. J Appl Phys 83:4389–4392. doi:10.1063/1.367198

Okada Y, Tokumaru Y (1984) Precise determination of lattice parameter and thermal expansion coefficient of silicon between 300 and 1500 K. J Appl Phys 56:314–321. doi:10.1063/1.333965

Ozgur U, YaI Alivov, Liu C, Teke A, Reshchikov MA, Doğan S, Avrutin V, Cho SJ, Morkoç H (2005) A comprehensive review of ZnO materials and devices. J Appl Phys 98:041301–041404. doi:10.1063/1.1992666

Raiko V, Spitzl R, Engermann J, Borisenko V, Bondarenko V (1996) MPCVD diamond deposition on porous silicon pretreated with the bias method. Diam Relat Mater 5:1063–1067. doi:10.1016/0925-9635(96)00514-6

Wang ZL (2004) Nanostructures of zinc oxide. Mater Today 7:26–33. doi:10.1016/S1369-7021(04)00286-X

Wang ZL (2008) Towards self-powered nanosystems: from nanogenerators to nanopiezotronics. Adv Funct Mat 18:3553–3567. doi:10.1002/adfm.200800541

Yakovtseva V, Vorozov N, Dolgyi L, Levchenko V, Postnova L, Balucani M, Bondarenko V, Lamedica G, Ferrara V, Ferrari A (2000) Porous silicon: a buffer layer for PbS heteroepitaxy. Phys Status Solidi (a) 182:195–199. doi:10.1002/1521-96X(200011)182:1<195:AID-PSSA195>3.0.CO;2-G

Zhang WC, Wu XL, Chen HT, Zhu J, Huang GS (2008) Excitation wavelength dependence of the visible photoluminescence from amorphous ZnO granular films. J Appl Phys 103:093718–093723. doi:10.1063/1.2924421